Crystalline Organic Pigment Based Field Effect Transistors

Haichang Zhang, Ruonan Deng, Jing Wang, Xiang Li, Yu-Ming Chen, Kewei Liu,

Clinton J Taubert, Stephen Z. D. Cheng and Yu Zhu*

Department of Polymer Science,

College of Polymer Science and Polymer Engineering,

The University of Akron,

170 University Circle, Akron, Ohio 44325-3909, United States

E-mail: yu.zhu@uakron.edu

ABSTRACT: Three conjugated pigment molecules with fused hydrogen-bonds, BDP (3,7-diphenylpyrrolo[2,3-*f*]indole-2,6(1*H*,5*H*)-dione), IIDG ((*E*)-6,6'-dibromo-[3,3'-biindolinylidene]-2,2'-dione), and TDPP (3,6-di(thiophen-2-yl)-2,5-dihydropyrrolo-[3,4-*c*]pyrrole-1,4-dione), were studied in this work. The insoluble pigment molecules were functionalized with *tert*-butoxylcarbonyl (*t*-Boc) groups to form soluble pigment precursors (BDP-Boc, IIDG-Boc and TDPP-Boc) with latent hydrogen bonding. The single crystals of soluble pigment precursors were obtained. Upon a simple thermal annealing, the *t*-Boc groups were removed and the soluble pigment precursor molecules with latent hydrogen bonding were converted into the original pigment molecules with fused hydrogen bonding. Structural analysis indicated that the highly crystalline soluble precursors were directly converted to highly crystalline insoluble pigments, which are usually only achievable by gas phase routes like physical vapor transport. The distinct

crystal structure after thermal annealing treatment suggests that fused hydrogen bonding is pivotal for the rearrangement of molecules to form new crystal in solid state, which leads to over two orders of magnitude enhancement in charge mobility in organic field effect transistor devices. This work demonstrated that crystalline OFET devices with insoluble pigment molecules can be fabricated by their soluble precursors. The results indicated that a variety of commercially available conjugated pigments could be potential active materials for high performance OFET.

Keywords: Hydrogen Bonding, Pigment, Crystal, Organic Field Effect Transistors, Latent Hydrogen Bonding

1. INTRODUCTION

The materials for the organic field effect transistors have been developed rapidly in the past two decades.[1] Among those materials, π-conjugated small molecules and polymers are the two most representative groups. However, although small molecules and polymers share certain similarities such as the conjugated structures and π-π stacking between molecules, the charge transport in those two types of organic semiconductors is distinctly different.[2-3] In small-molecule organic semiconductors, the charge carriers need to be frequently transferred between individual molecules, therefore the molecular packing and crystal size are crucial for efficient charge transport. Small molecules that form perfect, thin crystals, such as rubrene[4-5] and pentacene[6-8] single crystals grown from vapor phase deposition, exhibited the highest mobility in the order of 40 $cm^2/v \cdot s$. The charge transport in π-conjugated polymers is much more complicate as the polymers are usually semicrystalline, whereas, the charge

carriers need to travel across both crystalline and amorphous regions. Therefore, charge mobility is not only governed by the crystallinity of the polymer film, but also determined by the connections between crystalline aggregates.[2] Recent development of high mobility π-conjugated polymers[9-16] has demonstrated similar performance to small-molecule single crystal OFET devices. Interestingly, many high performance polymers have very different chemical structure from high performance small molecules. For example, two very successful repeat units in polymers, the pigment molecules isoindigo and diketopyrrolopyrrole, have lactam groups surmounting their aromatic ring. These polar groups generate strong molecular dipoles and were avoided in the early design of small-molecule semiconductors because the initial ideas regarding organic semiconductor materials sought to maximize π-conjugation. [17-18] Compared with acenes and thienoacenes, small molecule semiconductive pigments have not been widely investigated, although their corresponding polymers with mobility over 10 $cm^2/v \cdot s$ were reported by different groups.[11, 13-14, 19-22] Most small-molecule OFET studies using pigment like molecules are based on oligomers[23-24] or modified pigments[25-33], where the assembly of the molecules is governed by pendant groups rather than hydrogen bonding and the π-stacking interplay of the original pigments. Nevertheless, a few recent reports using pigments as small-molecule OFET materials exhibited the potentiality of this class of materials. The small-molecule OFET using diketopyrrolopyrrole pigment was firstly reported by Yanagisawa and coworkers.[34] The OFET devices prepared by both vacuum sublimation and spin-coating soluble precursors exhibited mobility in the range of 10^{-5} $cm^2/v \cdot s$. The vacuum deposition

method was improved in a recent report and the mobility achieved the range of 0.01-0.06 $cm^2/v \cdot s$.[35] Considering the simplicity of this molecule, the improvement of mobility is quite impressive. An oligomer DPP pigment OFET exhibited a similar performance (~ 6×10^{-3} $cm^2/v \cdot s$).[36] Isoindigo and its derivative pigment based OFET have been reported by T. Mori and co-workers; the OFET devices were prepared by vacuum deposition method which exhibited ambipolar properties with mobility between 7.2×10^{-3} $cm^2/v \cdot s$ and 0.037 $cm^2/v \cdot s$.[37] A similar pigment, indigo, has been reported recently[38-40] and exhibited the ambipolar charge transport behavior with mobility up to 0.01 $cm^2/v \cdot s$. Furthermore, the indigo derivative, epindolidione, has been reported to reach hole mobility of 1.5 $cm^2/v \cdot s$ after optimizing the dielectric materials in the devices.[41] Most reports on hydrogen bonded pigment molecules[34-36, 38-40, 42] studied the thin film, where the materials are in amorphous or highly disordered polycrystalline states. The research of crystalline pigment OFET device is very limited, possibly due to insolubility nature of most pigment molecules. Here in this report, three pigment molecules (BDP, IIDG and TDPP, **Figure 1**) were investigated in crystalline pigment OFET devices. These molecules and their derivative were widely used in coating industry and can be potentially low-cost active materials for organic electronics. The research is focused on the pigment molecules with fused hydrogen bonding (hydrogen bonding donor and acceptor units are within the π-conjugated structure) due to the following two reasons/assumptions: first, strong hydrogen bonding and π-stacking results in high crystal lattice energies, which are essential for the thermal- and photo-stability of many commercial organic pigments, allowing them to survive over

years under ambient conditions.[43-44] Thus the utilization of commercial pigments may be desired for organic electronics in the context of stability and cost. Second, the interplay of hydrogen bonding and π-stacking is well-known strategy for pigment crystal engineering to achieve the desired optical and mechanical properties.[45-46] These crystal engineering capabilities provided by the fused hydrogen bonding[40, 42, 47] may be important for small-molecule OFET device.

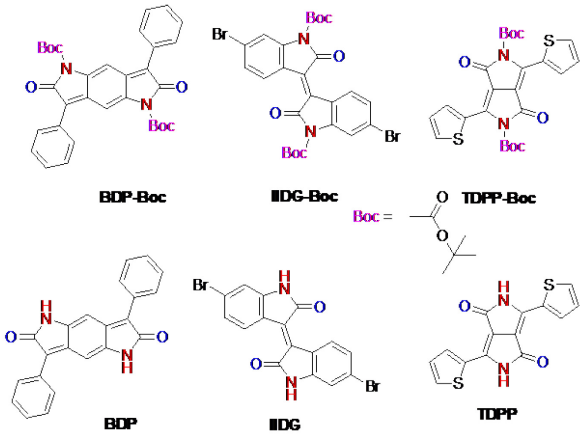

Figure 1. Structures of soluble pigment precursors (top row) and insoluble pigment (bottom row)

The commercial pigments with fused hydrogen bonding are typically insoluble due to the high crystal lattice energy, which prevents the growth of large pigment crystals in solution for OFET devices. In this method, a labile group (*t*-Boc) was introduced to block the hydrogen bonding formation. The pigments with *t*-Boc group are soluble in organic solvents and can be converted back to the hydrogen bonded pigment by thermal annealing. This "latent hydrogen bonding" was firstly reported on diketopyrrolopyrrole pigments.[48] It was recently used in several conjugated polymers to form latent hydrogen bonding based polymers.[49-51] As the crystallinity is pivotal for small molecule OFET devices, a crystal-to-crystal transition method was developed in

this work to fabricate crystalline pigment OFET devices. The single crystals of soluble pigment precursors were obtained by slow evaporation, upon a simple thermal annealing procedure, the solubilizing groups were removed and the soluble pigment precursors with latent hydrogen bonding were converted into the original pigment molecules with fused hydrogen bonding. Structure analysis indicated that the highly crystalline soluble pigments were directly converted to highly crystalline insoluble pigment during this process. The crystalline pigment OFET devices were then fabricated and measured.

2. RESULTS AND DISCUSSION

2.1 Synthesis and Conversion of Pigments and Soluble Precursors

The pigment molecules, BDP, IIDG and TDPP (**Figure 1**) were synthesized based on the previous reports (see supporting information, SI).[52-58] They all contain lactam units that can form intermolecular hydrogen bonding pairs (N–H···O=C, **Figure S1**). These strong intermolecular hydrogen bonding pairs render the small molecules insoluble in most solvents as well as contribute a high thermal- and photo- stability. The synthesis of *t*-Boc substituted precursors is described in the SI, following from the previous research.[48-51] After thermal annealing, the soluble precursors are converted to pigment with fused hydrogen bonding. (**Figure S2**) To validate the formation of pigments with fused hydrogen bonding after the decarboxylation of the *t*-Boc units, TGA, NMR and FTIR experiments were conducted. **Figure 2** shows the results of BDP. TDPP and IIDG results are included in the SI. As shown in **Figure 2a**, the deprotection of *t*-Boc group from BDP-Boc starts between 140 ºC and 180 ºC, depending on the

heating rate (1 ºC/min to 50 ºC/min). The weight loss is around 37.1 %, which matches well with weight percentage of *t*-Boc units in BDP-Boc (37.3 %). Similar TGA results were observed for TDPP-Boc and IIDG-Boc (**Figure S3**). The detailed deprotection process of *t*-Boc groups was followed by ^{1}H-NMR spectra. The results of BDP-Boc are shown in **Figure 2b**. In this experiment, the BDP-Boc samples were isothermally annealed at 140 ºC for different periods of time and then dissolved in DMSO-d6 for ^{1}H-NMR spectra. As shown in **Figure 2b**, the single peak chemical shift at 1.52 ppm (*t*-Boc methyl) decreases, splits into two smaller peaks (after heated for 1 h), and eventually disappears (after 48 h). Meanwhile new peaks (N-H) emerge at 10.21 and 10.49 ppm (1-10 h), and finally at 10.21 ppm (48 h). The NMR spectrum of the original BDP pigment exhibits the same signals as the NMR spectrum of BDP-Boc after thermal annealing for 48 hours. These observations are consistent with TGA results and the intermediate states (with multiple peaks for N-H) can be ascribed as the mixture of BDP pigments and monosubstituted BDP-Boc. ^{1}H-NMR spectra of IIDG-Boc to IIDG transition are shown in **Figure S4**. ^{1}H-NMR spectra of TDPP-Boc to TDPP transition are not available because TDPP is completely insoluble.

To further verify the formation of hydrogen-bonding, kinetic FTIR experiments were conducted during the annealing process of soluble pigment precursors. **Figure 2c** shows the results of BDP. The TDPP and IIDG results are shown in **Figures S5** and **S6**, respectively. As shown in **Figure 2c**, the kinetic FTIR data clearly indicate that strong hydrogen bonding-associated materials are formed in the solid state after annealing based on the following observations: i) the absorption peak at 1780 cm^{-1} (C=O

stretching of *t*-Boc group, yellow band) disappears after annealing; ii) a broad band absorption of 2600-3400 cm^{-1} emerges (green band), which is attributed to the hydrogen-bonded N-H stretching vibration; iii) the emerged peak of 1610 cm^{-1} which also indicates the formation of N-H (N-H bending) iv) the amide I band (C=O stretching, 1681 cm^{-1}, red band) and amide II band (N-H bending, 1610 cm^{-1} and C-N stretching, 1580 cm^{-1}, blue band) which confirms the formation of an amide with a secondary amine; and v) the shift of the carbonyl stretching (from 1730 cm^{-1} to 1681 cm^{-1} after annealing) is resultant of the change of the isolated carbonyl group on BDP into hydrogen bonded carbonyl group (N-H···O=C). The kinetic FTIR results agree very well with reported hydrogen bonding based systems.[59-63] Similar FTIR results were observed in TDPP and IIDG (**Figure S5** and **S6**).

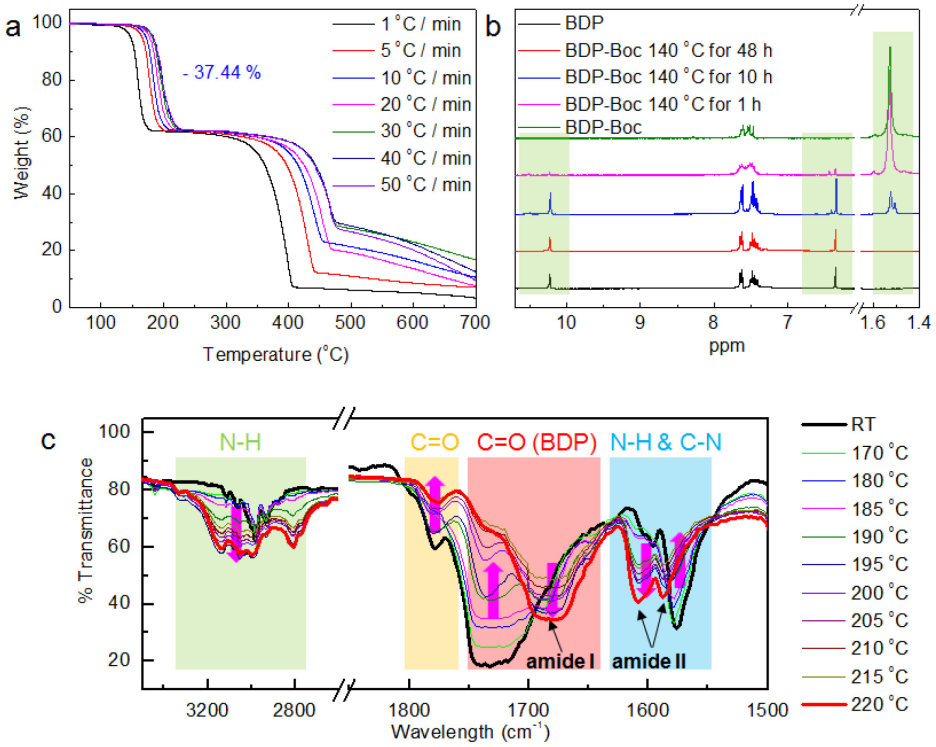

Figure 2. (a) TGA spectra of BDP-Boc with different heating rate indicated. (b) ^{1}H-NMR spectra of BDP-Boc isothermally annealed at 140 °C for 1h, 10h and 48 h, BDP-

Boc and BDP (solvent: DMSO-d6). (c) Kinetic FTIR spectra of BDP-Boc during thermal annealing process.

2.2 Crystal-to-Crystal Transition in Solid State

Highly crystalline materials are pivotal for small-molecule OFETs. In the initial tests, the uniform thin films of soluble pigment precursors were prepared on the surface of silicon wafer by spin-coating. The film was annealed at 200 ºC and the optical and SEM images, before and after annealing, were collected in **Figures S7-S9**. It is clear from the polarized optical images and subsequent SEM images that microcrystals are formed in this process. Those microcrystals are crystals of pigment molecules, as the temperature is high enough to eliminate the *t*-Boc units. Similar crystallization processes were reported previously for DPP oligomers,[64] though the size of the crystals were in the range of a few hundreds of nanometers. DSC experiments were conducted for all three soluble pigment precursors (**Figures S10-S12**). In the first scan, an exothermal peak was observed between 150 ºC and 210 ºC, which can be attributed to the cleavage *t*-Boc unit. In the following cycles, there is no peak observed between 25 ºC and 270 ºC, which is consistent with the high crystal lattice energy of hydrogen bonded pigment. Based on those observations, it is speculated that there was a crystallization process mostly driven by hydrogen bonding when the *t*-Boc group was being removed. This can be further explained as the following: when the *t*-Boc groups are removed, hydrogen bonding donor units (N-H) are generated. Before the donor units coordinate with the acceptor units (C=O) to form hydrogen bonding, the molecules are still mobile due to elevated temperature and relatively weak intermolecular interaction.

Therefore, the molecules may undergo a crystallization process to facilitate formation of hydrogen bonded crystals. Once the hydrogen bonded crystals were formed, the crystal lattice energy increased significantly, thus no melting process was observed in the same range of temperature.

Based on the results in DSC and thin film samples, a possible crystal-to-crystal transition in solid state is sought during the *t*-Boc removal process. Slow evaporation method was then used to grow the soluble pigment precursor crystals. The crystal samples were heated at different temperatures and then observed under a polarized optical microscope. Conventional optical images and the polarized optical images were recorded. **Figure 3a** shows a cluster of TDPP-Boc crystals (formed by slow evaporation of drop-casted TDPP-Boc solution on silicon wafer) and a large single IIDG-Boc crystal (formed by slow evaporation of IIDG-Boc dichloromethane/ethanol mixture) during this transition. Additional images are shown in **Figures S13-S16**. It can be seen in the optical images that the color of the crystal, as well as the roughness of the crystal surface, were changed during annealing. Despite those changes, the shape of the crystals remained intact throughout the annealing treatment. The drop-casting method provides the crystals with a size over a few hundreds of micrometers (**Figure 3a**, **Figure S13** and **Figure S14**) on the surface of a silicon wafer, which is large enough to fabricate a crystalline OFET device. The single crystal (**Figure 3a**, **Figure S15** and **Figure S16**) grown from dichloromethane/ethanol mixture reached a size over 1 millimeter, which allows X-ray diffraction experiments. The 1D XRD spectra of three soluble pigment precursors were collected and compared in **Figure 3b to 3d**. It is clear that the crystal

structures were changed after thermal annealing in this case. All XRD spectra have sharp peaks, indicating a crystal-to-crystal transition in solid state. To further understand the structure of the crystal after annealing, crystals of insoluble pigments (BDP, TDPP and IIDG) were grown by physical vapor transport (PVT) technique.[65] The 1D XRD spectra of PVT crystals are shown in **Figure 3b to 3d** as well (blue curves). The XRD patterns of PVT crystals match very well with the XRD patterns of annealed soluble pigment precursors. **Figure 3e** shows the XRD spectra of TDPP-Boc samples annealed under different temperatures. The XRD spectra have sharp peaks under different temperatures, indicating a direct crystal-to-crystal transition in solid state. Such a transition process is similar as topochemical and topotactic reactions.[66] However, topochemical and topotactic reactions typically involve the formation of covalent linking. In this work, the new intermolecular interaction (hydrogen bonding) is formed. These results confirm that the crystalline soluble pigment precursors are converted to crystalline hydrogen bonded pigments during the *t*-Boc elimination process.

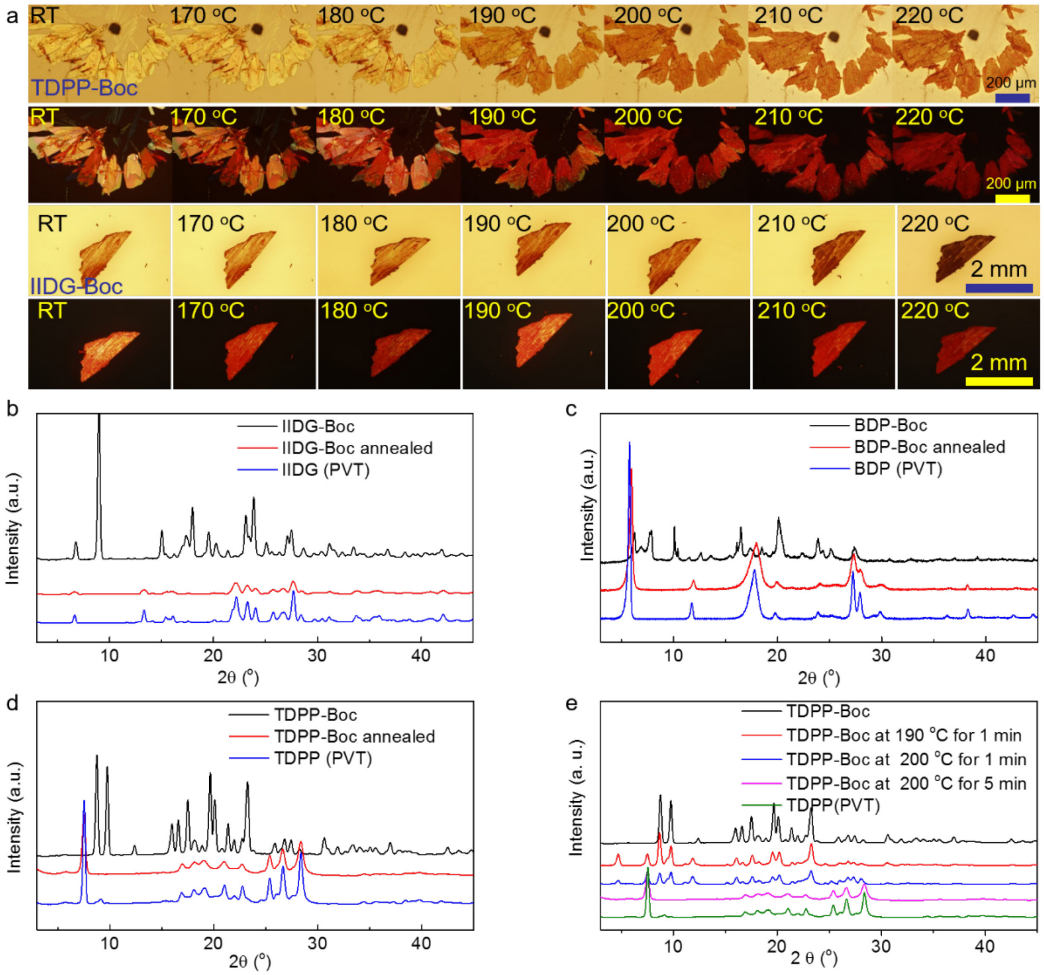

Figure 3. (a) Conventional optical images (first row) and polarized optical images (second row) of TDPP-Boc crystal clusters obtained through drop-casting/slow evaporation method. The images show the crystal-to-crystal transition during the annealing process. The third row (conventional optical images) and the fourth row (polarized optical images) is the crystal transition process of a IIDG-Boc crystal grown from dichloromethane/ethanol mixture. (b to d) 1D XRD spectra of BDP, IIDG and TDPP derivatives as indicated. black line: soluble precursor crystal prepared by slow evaporation in solution; red line: soluble precursor crystal after thermal annealing (converted insoluble pigment crystal); blue line: insoluble pigment crystal prepared by physical vapor transport technique. (e) 1D XRD spectra of TDPP-Boc at different

annealing conditions. The TDPP-Boc samples was annealed under different temperatures for a period of time (as indicated). The 1D XRD spectrum of **TDPP** crystal grown by PVT method is listed in the figure for comparison.

The transition from soluble pigment precursor crystal to hydrogen bonded pigment crystal is accompanied with a drastic change on optical properties. All hydrogen bonded pigments exhibited a red-shift on UV/Vis absorption spectra as compared to their soluble precursors (**Figures S17-S19**). The bathochromic shift can be attributed to the removal of the *t*-Boc group and the formation of the hydrogen bonding, resulting in molecules with better coplanarity and tighter packing. The single crystal structures of IIDG-Boc[67] and IIDG (PVT) are shown in **Figure 4**. The IIDG-Boc crystal is orthorhombic with space group of $Pca2_1$, [67] while the IIDG crystal is triclinic with space group of P1. In the IIDG-Boc crystal, the center chromophore is twisted and the dihedral angle of the two twisted oxindole rings is 25.5 º (**Figure 4a**). In the IIDG crystal, the dihedral angle is only 13.3 º (**Figure 4d**). This indicates that the original pigment, IIDG, has a better coplanar structure. The π-π stacking distances in IIDG-Boc and IIDG crystals are similar (IIDG-Boc: 3.38 Å, IIDG: 3.30 Å, **Figure 4b** and **4e**, respectively); however, hydrogen bonding exists only in in the IIDG crystal. As illustrated in **Figure 4f**, the adjacent IIDG molecules are connected by a pair of hydrogen bonds (N-H···O=C). The lengths of the two hydrogen bonds are slightly different, with the stronger one having N-O distance of 2.80 Å, H-O distance of 1.93 Å, N-H-O angle of 170 º and the slightly weaker one having N-O distance of 2.85 Å, H-O distance of 1.99 Å, N-H-O angle of 163 º. Although both hydrogen bonds are not linear,

the connected two oxindole rings are within the same plane. The existence of hydrogen bonding leads to a completely different molecule packing in IIDG crystal. As shown in **Figure 4g**, the IIDG molecules form brick-wall packing with hydrogen bonding connecting adjacent IIDG molecules as a layered structure (the torsion angle of adjacent C-N⋯⋯C-N is close to 0°). The π-π stacking direction is perpendicular to the hydrogen bonded plane. In contrast, the packing of IIDG-Boc (**Figure 4c**) is mainly governed by Van der Waals forces and π-π stacking, resulting in a herringbone structure. The π-π stacking distance in IIDG-Boc is slightly larger than that of IIDG and the distance between the adjacent molecules is significantly larger than the hydrogen bonded IIDG.

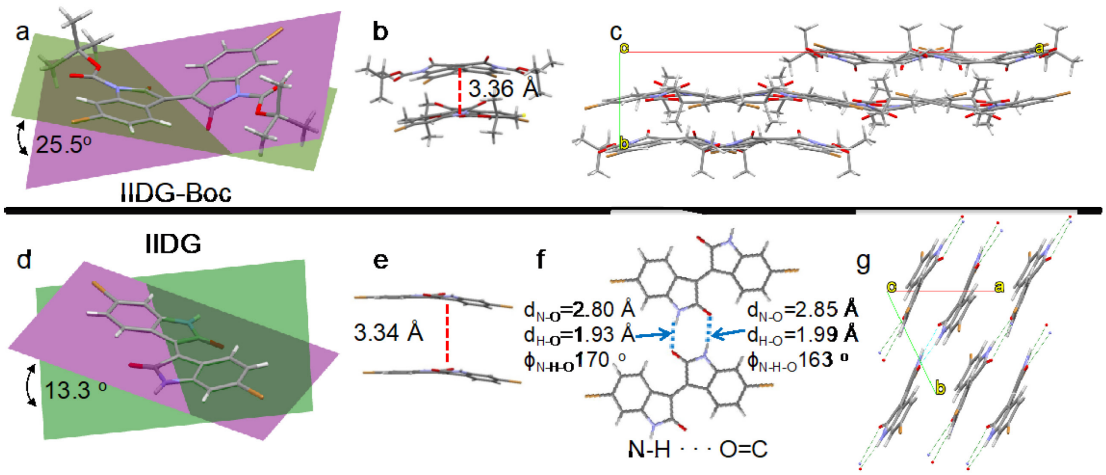

Figure 4. Single crystal structure of IIDG-Boc and IIDG (a, d) the dihedral angles of two oxindole rings in IIDG-Boc and IIDG. (b, e) The π-π stacking distance for IIDG-Boc and IIDG crystals. (c) The herringbone packed IIDG-Boc crystal (viewing from the c axis). (f) The detailed hydrogen bonded structure in IIDG. A pair of hydrogen bonds are formed between the adjacent IIDG molecules. The length and the angle of the hydrogen bonds are illustrated in the figure. The two oxindole rings connected by the hydrogen bonding are in the same plane. (g) The brick-wall packed IIDG crystal

(viewing from the c axis).

2.3 OFET Devices

Although the soluble precursor lost ~ 30% weight during the annealing process, the crystal-to-crystal transition reserved the morphology of the crystal samples. The crystal samples were examined under SEM to evaluate the change of the crystal sizes. **Figure 5** show the SEM images of the crystals before and after annealing. The densities of IIDG-Boc and IIDG are 1.566 g/cm^3 and 1.692 g/cm^3, respectively. Based on the molecular weights of IIDG-Boc and IIDG, the volume of the crystal shrinks to 0.6268 if the original size is unit. Assuming the size change of the crystal is isotropic (the size on the three crystal directions changes in the same ratio), the area of the crystal will shrink to 73.2% of its original size. As shown in the SEM images in **Figures 5a and 5d**, the area of the crystal is integrated and the shrinkage of the crystal area is 77.7%. The difference between the calculated value and measured result can be explained as the anisotropic change of crystal size. Similar crystal shrinkage was observed in TDPP and BDP crystals (**Figures 5b, 5e** and **5c, 5f**) and the area of the crystal shrink to 79.5% and 80.7% for TDPP and BDP, respectively. The shrinkage of the entire crystal, instead of exploding the original crystal, can be attributed to the recrystallization process appeared during the decarboxylation. Such a crystal-to-crystal transition in solid state allows the fabrication of crystalline OFETs of insoluble pigments from their soluble precursor crystal.

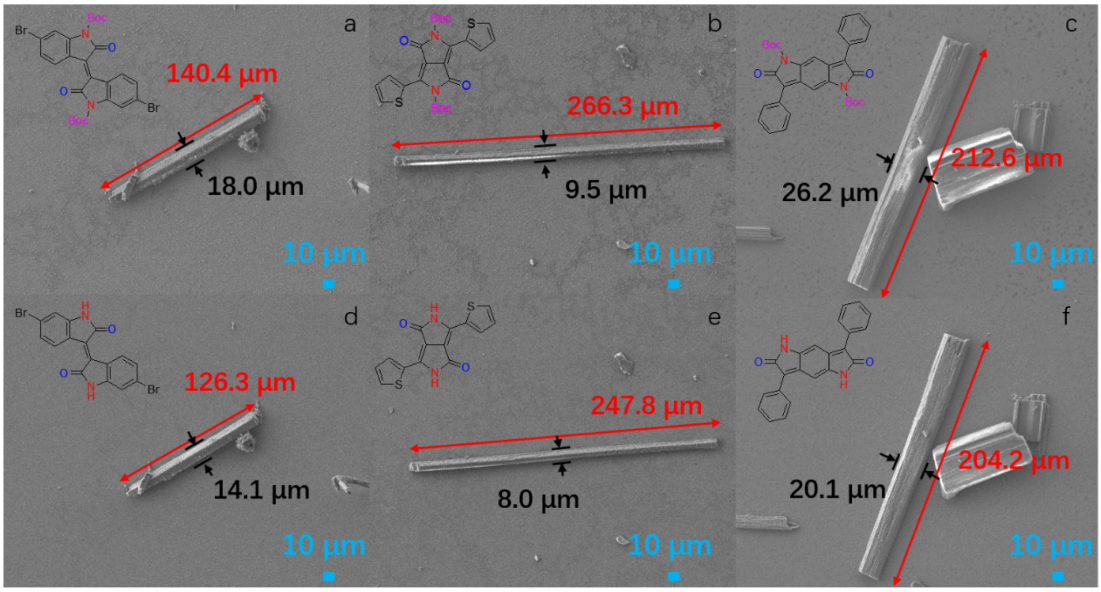

Figure 5. SEM images of IIDG-Boc, TDPP-Boc, BDP-Boc crystals before (a, b and c) and after (d, e and f) thermal annealing. The crystal area changes during the thermal annealing are from 2213.5 μm^2 to 1718.8 μm^2 for IIDG-Boc (area change: 77.7 %), from 2597.1 μm^2 to 2065.7 μm^2 for TDPP-Boc (area change: 79.5 %), from 5000.4 μm^2 to 4036.9 μm^2 for BDP-Boc (area change: 80.7 %), respectively. The representative length and width changes of the crystal size are indicated in the figures.

In order to fabricate the OFET device, the same method to generate thin crystals on silicon wafers in **Figure 3a** was used. The crystals of soluble precursors (BDP-Boc, IIDG-Boc and TDPP-Boc) were directly grown on the silicon wafer with pre-patterned source and drain electrodes. The details of device fabrication are described in SI. **Figures 6a**, **6c** and **6b**, **6d** are optical images of TDPP-Boc device under conventional mode and polarized mode, respectively. The device was then annealed to convert the TDPP-Boc crystal to a TDPP crystal. The optical images of converted TDPP crystals are shown in **Figures 6e-6h**. It is very clear that the crystal is shining under polarized

microscope throughout the annealing treatment, suggesting highly crystalline pigment sample after decarboxylation. The same device was measured before and after thermal annealing to compare the charge transport properties of the precursors and pigments. **Figures 6i-l** show the results of TDPP-Boc and TDPP. The results of BDP and IIDG are shown in SI **Figures S20-S21**. The OFET characteristics of the compounds are summarized in Table S1. All three pigments and their soluble precursors showed p-type behavior. The hole mobility was enhanced from 2.6 $\times 10^{-3}$ $cm^2/v \cdot s$ to 0.26 $cm^2/v \cdot s$ for TDPP; 8.5 $\times 10^{-3}$ $cm^2/v \cdot s$ to 0.14 $cm^2/v \cdot s$ for IIDG; and from 1.8×10^{-3} $cm^2/v \cdot s$ to 0.084 $cm^2/v \cdot s$ for BDP (**Figure 6 i-l**, **Figure S20 i-l** and **Figure S21 i-l**) Based on the structure information of IIDG, the significant enhancement of the hole mobility could be explained as the changing of solid state structure in such that: i) the dihedral angle of the two oxindole rings was significantly reduced from 25.5° to 13.3° after the *t*-Boc elimination, which enhanced the coplanarity of the molecules. ii) hydrogen-bonding emerged between the carbonyl group (C=O) and the amine group (N-H) of the neighboring IIDG molecules, resulting in a stronger intermolecular interactions and increased molecule core density from 1.566 $g \cdot cm^{-3}$ (IIDG-Boc) to 1.692 $g \cdot cm^{-3}$ (IIDG). iii) the π-π stacking was slightly changed from 3.38 Å to 3.30 Å after thermal annealing. All together, the hole mobility was enhanced nearly 100 fold after the crystal-to-crystal transition for TDPP, 47 fold for BDP, and 16 fold for IIDG. Compared with other similar work of hydrogen bonded small molecules, the reported OFETs performance in this work is among the highest (Table S2).

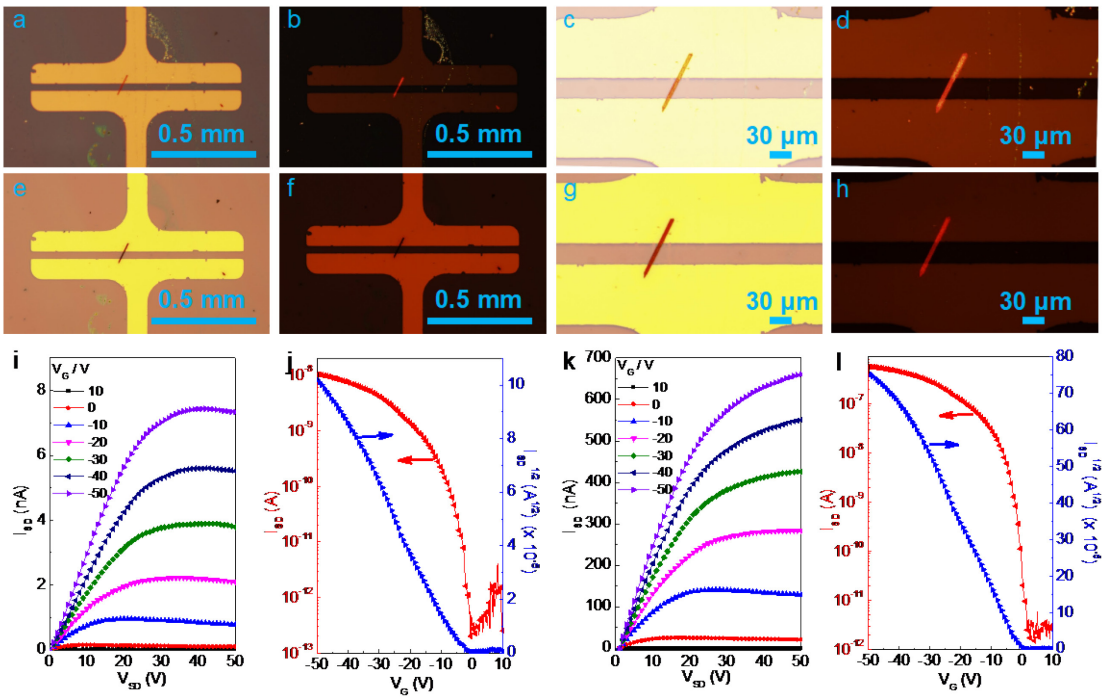

Figure 6. OFET characteristics of TDPP-Boc. (a, c) Conventional optical images of TDPP-Boc device. (b, d) Polarized optical images of TDPP-Boc device. The width of the crystal is 6.90 μm. (e, g) Conventional optical images of annealed device. (f, h) Polarized optical image of annealed device. The width of the crystal is 6.65 μm. (i) The output characteristics of TDPP-Boc device. (j) The transfer characteristics of TDPP-Boc device. (k) The output characteristics of annealed device measured at V_D = -40 V (l) The transfer characteristics of annealed device measured at V_D = -40 V.

3. CONCLUSION

In summary, three small molecules BDP, IIDG and TDPP with fused hydrogen-bonds are investigated. The *t*-Boc substituted soluble precursors can be decarboxylated and will subsequently form the original insoluble pigments with fused hydrogen bonding. A solid state crystal-to-crystal transition was observed during the

decarboxylation process. The crystal structures of the annealed precursors are same as that of pigments crystal grown by PVT method. The uniqueness of this crystal-to-crystal transition is that it only happens during the *t*-Boc elimination process, given the fact that the pigment crystal has high crystal lattice energy and can not be melted once formed (under the temperature range of DSC experiments conducted). The size of the pigment crystal depends on the initial states of the precursor: a uniform thin precursor film generates microcrystals while a large single crystal precursor results in a large pigment crystal. The formation of the hydrogen bonding in the pigment crystal is confirmed by both kinetic FTIR and single crystal X-Ray data. This crystal transition also leads to a dramatic change in optical and electronic properties. Hydrogen bonded pigments exhibited bathochromic shift on UV/Vis spectra and 1-2 orders of magnitude higher hole mobility, up to 0.26 $cm^2/v \cdot s$. Such an enhancement can be attributed to the better coplanar structure of the chromophore and more densely packed molecules from hydrogen bonding. More intriguingly, the fused hydrogen bond may be used for achieving desired molecule packing, as indicated in the IIDG crystal. This opens a new route to study a variety of conjugated pigments (such as DPP and IIDG) which, due to possessing a large dipole moment, were much less investigated than acenes and thienoacenes, even though their polymers have been proved to be excellent organic semiconductors.

Corresponding Author

* Yu Zhu. E-mail: yu.zhu@uakron.edu

Author Contributions All authors have given approval to the final version of the manuscript.

Conflict of Interest The authors declare no competing financial interest.

Acknowledgements The authors thank E. Laughlin for technical support. This work is supported by the National Science Foundation (DMR-1554851). Part of the work is supported by the CBET-1505943 and CBET-1336057, ACS Petroleum Research Fund (PRF# 53560 -DNI 10) and DOE STTR (DE-SC0013831).

Supporting Information Available Additional NMR, TGA, DSC and materials synthesis procedures. These materials are available free of charge *via* the Internet at http://pubs.acs.org.

REFERENCES

(1) Klauk, H. Organic Thin-Film Transistors. *Chem. Soc. Rev.* **2010**, *39*, 2643-2666.

(2) Noriega, R.; Rivnay, J.; Vandewal, K.; Koch, F. P. V.; Stingelin, N.; Smith, P.; Toney, M. F.; Salleo, A. A General Relationship Between Disorder, Aggregation and Charge Transport in Conjugated Polymers. *Nat. Mater.* **2013**, *12*, 1038-1044.

(3) Coropceanu, V.; Cornil, J.; da Silva Filho, D. A.; Olivier, Y.; Silbey, R.; Brédas, J.-L. Charge Transport in Organic Semiconductors. *Chem. Rev.* **2007**, *107*, 926-952.

(4) Sundar, V. C.; Zaumseil, J.; Podzorov, V.; Menard, E.; Willett, R. L.; Someya, T.; Gershenson, M. E.; Rogers, J. A. Elastomeric Transistor Stamps: Reversible Probing of Charge Transport in Organic Crystals. *Science* **2004**, *303*, 1644-1646.

(5) Takeya, J.; Kato, J.; Hara, K.; Yamagishi, M.; Hirahara, R.; Yamada, K.; Nakazawa, Y.; Ikehata, S.; Tsukagoshi, K.; Aoyagi, Y. In-Crystal and Surface Charge Transport of Electric-Field-Induced Carriers in Organic Single-Crystal Semiconductors. *Phys. Rev. Lett.* **2007**, *98*, 196804.

(6) Jurchescu, O. D.; Popinciuc, M.; van Wees, B. J.; Palstra, T. T. M. Interface-Controlled, High-Mobility Organic Transistors. *Adv. Mater.* **2007**, *19*, 688-692.

(7) Takeya, J.; Goldmann, C.; Haas, S.; Pernstich, K. P.; Ketterer, B.; Batlogg, B. Field-Induced Charge Transport at the Surface of Pentacene Single Crystals: A Method to Study Charge Dynamics of Two-Dimensional Electron Systems in Organic Crystals. *J. Appl. Phys.* **2003,** *94*, 5800-5804.

(8) Goldmann, C.; Haas, S.; Krellner, C.; Pernstich, K. P.; Gundlach, D. J.; Batlogg, B. Hole Mobility in Organic Single Crystals Measured by A “Flip-Crystal” Field-Effect Technique. *J. Appl. Phys.* **2004**, *96*, 2080-2086.

(9) Lei, T.; Cao, Y.; Fan, Y.; Liu, C.-J.; Yuan, S.-C.; Pei, J. High-Performance Air-Stable Organic Field-Effect Transistors: Isoindigo-Based Conjugated Polymers. *J. Am. Chem. Soc*. **2011**, *133*, 6099-6101.

(10) Mei, J.; Kim, D. H.; Ayzner, A. L.; Toney, M. F.; Bao, Z. Siloxane-Terminated Solubilizing Side Chains: Bringing Conjugated Polymer Backbones Closer and Boosting Hole Mobilities in Thin-Film Transistors. *J. Am. Chem. Soc*. **2011**, *133*, 20130-20133.

(11) Kim, G.; Kang, S.-J.; Dutta, G. K.; Han, Y.-K.; Shin, T. J.; Noh, Y.-Y.; Yang, C. A Thienoisoindigo-Naphthalene Polymer with Ultrahigh Mobility of 14.4 cm2/V·s That

Substantially Exceeds Benchmark Values for Amorphous Silicon Semiconductors. *J. Am. Chem. Soc.* **2014**, *136*, 9477-9483.

(12) Bronstein, H.; Chen, Z.; Ashraf, R. S.; Zhang, W.; Du, J.; Durrant, J. R.; Shakya Tuladhar, P.; Song, K.; Watkins, S. E.; Geerts, Y.; Wienk, M. M.; Janssen, R. A. J.; Anthopoulos, T.; Sirringhaus, H.; Heeney, M.; McCulloch, I. Thieno[3,2-b]thiophene-Diketopyrrolopyrrole-Containing Polymers for High-Performance Organic Field-Effect Transistors and Organic Photovoltaic Devices. *J. Am. Chem. Soc.* **2011**, *133*, 3272-3275.

(13) Chen, H.; Guo, Y.; Yu, G.; Zhao, Y.; Zhang, J.; Gao, D.; Liu, H.; Liu, Y. Highly π-Extended Copolymers with Diketopyrrolopyrrole Moieties for High-Performance Field-Effect Transistors. *Adv. Mater.* **2012**, *24*, 4618-4622.

(14) Liu, X.; Guo, Y.; Ma, Y.; Chen, H.; Mao, Z.; Wang, H.; Yu, G.; Liu, Y. Flexible, Low-Voltage and High-Performance Polymer Thin-Film Transistors and Their Application in Photo/Thermal Detectors. *Adv. Mater.* **2014,** *26*, 3631-3636.

(15) Shin, J.; Hong, T. R.; Lee, T. W.; Kim, A.; Kim, Y. H.; Cho, M. J.; Choi, D. H. Template-Guided Solution-Shearing Method for Enhanced Charge Carrier Mobility in Diketopyrrolopyrrole-Based Polymer Field-Effect Transistors. *Adv. Mater.* **2014**, *26*, 6031-6035.

(16) Choi, H. H.; Baek, J. Y.; Song, E.; Kang, B.; Cho, K.; Kwon, S.-K.; Kim, Y.-H. A Pseudo-Regular Alternating Conjugated Copolymer Using an Asymmetric Monomer: A High-Mobility Organic Transistor in Nonchlorinated Solvents. *Adv. Mater.* **2015**, *27*, 3626-3631.

(17) Facchetti, A. π-Conjugated Polymers for Organic Electronics and Photovoltaic Cell Applications. *Chem. Mater*. **2011**, *23*, 733-758.

(18) Pron, A.; Rannou, P. Processible Conjugated Polymers: From Organic Semiconductors to Organic Metals and Superconductors. *Prog. Polym. Sci.* **2002**, *27*, 135-190.

(19) Li, Y.; Singh, S. P.; Sonar, P., A High Mobility P-Type DPP-Thieno[3,2-b]thiophene Copolymer for Organic Thin-Film Transistors. *Adv. Mater.* **2010,** *22*, 4862-4866.

(20) Li, J.; Zhao, Y.; Tan, H. S.; Guo, Y.; Di, C.-A.; Yu, G.; Liu, Y.; Lin, M.; Lim, S. H.; Zhou, Y.; Su, H.; Ong, B. S., A Stable Solution-Processed Polymer Semiconductor with Record High-Mobility for Printed Transistors. *Sci. Rep.* **2012,** *2*, 754.

(21) Kang, I.; Yun, H.-J.; Chung, D. S.; Kwon, S.-K.; Kim, Y.-H., Record High Hole Mobility in Polymer Semiconductors via Side-Chain Engineering. *J. Am. Chem. Soc.* **2013,** *135*, 14896-14899.

(22) Back, J. Y.; Yu, H.; Song, I.; Kang, I.; Ahn, H.; Shin, T. J.; Kwon, S.-K.; Oh, J. H.; Kim, Y.-H., Investigation of Structure–Property Relationships in Diketopyrrolopyrrole-Based Polymer Semiconductors via Side-Chain Engineering. *Chem. Mater.* **2015,** *27*, 1732-1739.

(23) Tantiwiwat, M.; Tamayo, A.; Luu, N.; Dang, X.-D.; Nguyen, T.-Q. Oligothiophene Derivatives Functionalized with A Diketopyrrolopyrrolo Core for Solution-Processed Field Effect Transistors: Effect of Alkyl Substituents and Thermal Annealing. *J. Phys. Chem. C* **2008**, *112*, 17402-17407.

(24) Zhang, Y.; Kim, C.; Lin, J.; Nguyen, T. Q. Solution-Processed Ambipolar Field-Effect Transistor Based on Diketopyrrolopyrrole Functionalized with Benzothiadiazole. *Adv. Funct. Mater.* **2012**, *22*, 97-105.

(25) Molinari, A. S.; Alves, H.; Chen, Z.; Facchetti, A.; Morpurgo, A. F. High Electron Mobility in Vacuum and Ambient For PDIF-CN_2 Single-Crystal Transistors. *J. Am. Chem. Soc.* **2009**, *131*, 2462-2463.

(26) Jones, B. A.; Facchetti, A.; Wasielewski, M. R.; Marks, T. J. Effects of Arylene Diimide Thin Film Growth Conditions on n-Channel OFET Performance. *Adv. Funct. Mater.* **2008**, *18*, 1329-1339.

(27) Jones, B. A.; Ahrens, M. J.; Yoon, M. H.; Facchetti, A.; Marks, T. J.; Wasielewski, M. R. High-Mobility Air-Stable n-Type Semiconductors with Processing Versatility: Dicyanoperylene-3, 4: 9, 10-bis (dicarboximides). *Angew*. *Chem. Int. Ed.* **2004**, *116*, 6523-6526.

(28) Suraru, S.-L.; Zschieschang, U.; Klauk, H.; Würthner, F. Diketopyrrolopyrrole As A P-Channel Organic Semiconductor For High Performance OFETs. *Chem. Commun.* **2011**, *47*, 1767-1769.

(29) Qiao, Y.; Guo, Y.; Yu, C.; Zhang, F.; Xu, W.; Liu, Y.; Zhu, D. Diketopyrrolopyrrole-Containing Quinoidal Small Molecules for High-Performance, Air-Stable, and Solution-Processable N-Channel Organic Field-Effect Transistors. *J. Am. Chem. Soc.* **2012**, *134*, 4084-4087.

(30) Lin, Y.; Cheng, P.; Li, Y.; Zhan, X. A 3D Star-Shaped Non-Fullerene Acceptor for Solution-Processed Organic Solar Cells with A High Open-Circuit Voltage of 1.18 V. *Chem. Commun.* **2012,** *48*, 4773-4775.

(31) He, T.; Stolte, M.; Würthner, F. Air-Stable n-Channel Organic Single Crystal Field-Effect Transistors Based on Microribbons of Core-Chlorinated Naphthalene Diimide. *Adv. Mater.***2013**, *25*, 6951-6955.

(32) He, T.; Stolte, M.; Burschka, C.; Hansen, N. H.; Musiol, T.; Kälblein, D.; Pflaum, J.; Tao, X.; Brill, J.; Würthner, F. Single-Crystal Field-Effect Transistors of New Cl2-NDI Polymorph Processed by Sublimation in Air. *Nat. Commun*. **2015**, 6, 5954.

(33) Yue, W.; He, T.; Stolte, M.; Gsanger, M.; Wurthner, F. Cyanated Isoindigos for N-Type and Ambipolar Organic Thin Film Transistors. *Chem. Commun.* **2014**, *50*, 45-547.

(34) Yanagisawa, H.; Mizuguchi, J.; Aramaki, S.; Sakai, Y. Organic Field-Effect Transistor Devices Based on Latent Pigments of Unsubstituted Diketopyrrolopyrrole Or Quinacridone. *Jpn. J. Appl. Phys*. **2008**, *47*, 4728.

(35) Głowacki, E. D.; Coskun, H.; Blood-Forsythe, M. A.; Monkowius, U.; Leonat, L.; Grzybowski, M.; Gryko, D.; White, M. S.; Aspuru-Guzik, A.; Sariciftci, N. S. Hydrogen-Bonded Diketopyrrolopyrrole (DPP) Pigments as Organic Semiconductors. *Org. Electron*. **2014,** *15*, 3521-3528.

(36) Suna, Y.; Nishida, J.-i.; Fujisaki, Y.; Yamashita, Y. Ambipolar Behavior of Hydrogen-Bonded Diketopyrrolopyrrole-Thiophene Co-oligomers Formed from Their Soluble Precursors. *Org. lett.* **2012**, *14*, 3356-3359.

(37) Ashizawa, M.; Masuda, N.; Higashino, T.; Kadoya, T.; Kawamoto, T.; Matsumoto,

H.; Mori, T., Ambipolar Organic Transistors Based on Isoindigo Derivatives. *Org. Electron*. **2016,** *35*, 95-100.

(38) Irimia-Vladu, M.; Głowacki, E. D.; Troshin, P. A.; Schwabegger, G.; Leonat, L.; Susarova, D. K.; Krystal, O.; Ullah, M.; Kanbur, Y.; Bodea, M. A. Indigo-A Natural Pigment for High Performance Ambipolar Organic Field Effect Transistors and Circuits. *Adv. Mater.* **2012**, *24*, 375-380.

(39) Głowacki, E.; Apaydin, D.; Bozkurt, Z.; Monkowius, U.; Demirak, K.; Tordin, E.; Himmelsbach, M.; Schwarzinger, C.; Burian, M.; Lechner, R. Air-Stable Organic Semiconductors Based On 6, 6′ -Dithienylindigo and Polymers Thereof. *J. Mater. Chem. C* **2014**, *2*, 8089-8097.

(40) Anokhin, D. V.; Leshanskaya, L. I.; Piryazev, A. A.; Susarova, D. K.; Dremova, N. N.; Shcheglov, E. V.; Ivanov, D. A.; Razumov, V. F.; Troshin, P. A. Towards Understanding the Behavior of Indigo Thin Films in Organic Field-Effect Transistors: A Template Effect of the Aliphatic Hydrocarbon Dielectric on the Crystal Structure and Electrical Performance of the Semiconductor. *Chem. Commun.* **2014**, *50*, 7639-7641.

(41) Głowacki, E. D.; Irimia-Vladu, M.; Kaltenbrunner, M.; Gsiorowski, J.; White, M. S.; Monkowius, U.; Romanazzi, G.; Suranna, G. P.; Mastrorilli, P.; Sekitani, T.; Bauer, S.; Someya, T.; Torsi, L.; Sariciftci, N. S. Hydrogen-Bonded Semiconducting Pigments for Air-Stable Field-Effect Transistors. *Adv. Mater.* **2013**, *25*, 1563-1569.

(42) Oh, J. H.; Lee, W.-Y.; Noe, T.; Chen, W.-C.; Könemann, M.; Bao, Z. Solution-Shear-Processed Quaterrylene Diimide Thin-Film Transistors Prepared by Pressure-Assisted Thermal Cleavage of Swallow Tails. *J. Am. Chem. Soc.* **2011**, *133*, 4204-4207.

(43) Faulkner, E. B.; Schwartz, R. J. E. High Performance Pigments. 2nd ed. Wiley-VCH; Weinheim:2009.

(44) Mizuguchi, J. Correlation Between Crystal and Electronic Structures in Diketopyrrolopyrrole Pigments as Viewed From Exciton Coupling Effects. *J. Phys. Chem. A* **2000**, *104*, 1817-1821.

(45) Desiraju, G. R. DESIRAJU: C-H … O Hydrogen Bonding and the Deliberate Design of Organic Crystal Structures. *Mol. Cryst. Liq. Cryst*. **1992**, *211*, 63-74.

(46) Desiraju, G. R. Crystal engineering. From Molecules to Materials. *J. Mol. Struct*. **2003**, *656*, 5-15.

(47) Gsänger, M.; Oh, J. H.; Könemann, M.; Höffken, H. W.; Krause, A. M.; Bao, Z.; Würthner, F. A Crystal-Engineered Hydrogen-Bonded Octachloroperylene Diimide with a Twisted Core: An n-Channel Organic Semiconductor. *Angew. Chem. Int. Ed*. **2010**, *49*, 740-743.

(48) Zambounis, J. S.; Hao, Z.; Iqbal, A. Latent Pigments Activated by Heat. *Nature* **1997**, *388*, 131-132.

(49) Yang, K.; He, T.; Chen, X.; Cheng, S. Z. D.; Zhu, Y. Patternable Conjugated Polymers with Latent Hydrogen-Bonding on the Main Chain. *Macromolecules* **2014**, *47*, 8479-8486.

(50) Berns, B.; Tieke, B. Electrochromic Polyiminocarbazolylenes with Latent Hydrogen Bonding. *Polym. Chem.* **2015**, *6*, 4887-4901.

(51) Bruni, F.; Sassi, M.; Campione, M.; Giovanella, U.; Ruffo, R.; Luzzati, S.; Meinardi, F.; Beverina, L.; Brovelli, S. Post-Deposition Activation of Latent Hydrogen-

Bonding: A New Paradigm for Enhancing the Performances of Bulk Heterojunction Solar Cells. *Adv. Funct. Mater.* **2014**, *24*, 7410-7419.

(52) Greenhalgh, C. W.; Carey, J. L.; Newton, D. F. The Synthesis of Quinodimethanes in the Benzodifuranone and Benzodipyrrolidone Series. *Dyes Pigm*. **1980**, *1*, 103-120.

(53) Cui, W.; Yuen, J.; Wudl, F. Benzodipyrrolidones and Their Polymers. *Macromolecules* **2011**, *44*, 7869-7873.

(54) Zhang, H.; Ghasimi, S.; Tieke, B.; Schade, A.; Spange, S. Aminobenzodione-Based Polymers with Low Bandgaps and Solvatochromic Behavior. *Polym. Chem.* **2014**, *5*, 3817-3823.

(55) Zhang, H.; Tieke, B. Conjugated Polymers Containing Benzo-and Naphthodione Units in the Main Chain. *Polym. Chem.* **2014**, *5*, 6391-6406.

(56) Stas, S.; Sergeyev, S.; Geerts, Y. Synthesis of Diketopyrrolopyrrole (DPP) Derivatives Comprising Bithiophene Moieties. *Tetrahedron* **2010**, *66*, 1837-1845.

(57) Zou, Y.; Gendron, D.; Badrou-Aïch, R.; Najari, A.; Tao, Y.; Leclerc, M. A High-Mobility Low-Bandgap Poly(2,7-carbazole) Derivative for Photovoltaic Applications. *Macromolecules* **2009**, *42*, 2891-2894.

(58) Mei, J.; Graham, K. R.; Stalder, R.; Reynolds, J. R. Synthesis of Isoindigo-Based Oligothiophenes for Molecular Bulk Heterojunction Solar Cells. *Org. lett.* **2010**, *12*, 660-663.

(59) Hu, Y.; Motzer, H.; Etxeberria, A.; Fernandez-Berridi, M.; Iruin, J.; Painter, P. C.; Coleman, M. M. Concerning the Self-Association of N-Vinyl Pyrrolidone and Its Effect

on the Determination Of Equilibrium Constants and the Thermodynamics of Mixing. *Macromol. Chem. Phys.* **2000**, *201*, 705-714.

(60) Kuo, S. W.; Chang, F. C. Studies of Miscibility Behavior and Hydrogen Bonding in Blends of Poly(vinylphenol) and Poly(vinylpyrrolidone). *Macromolecules* **2001**, *34*, 5224-5228.

(61) Coleman, M. M.; Skrovanek, D. J.; Hu, J.; Painter, P. C. Hydrogen Bonding in Polymer Blends. 1. FTIR Studies of Urethane-Ether Blends. *Macromolecules* **1988**, *21*, 59-65.

(62) Garcia, D.; Starkweather, H. W. Hydrogen Bonding in Nylon 66 and Model Compounds. *J. Polym. Sci. Part B: Polym. Phys.* **1985**, *23*, 537-555.

(63) Macknight, W. J.; Yang, M. Property-Structure Relationships in Poly-Urethanes: Infrared Studies. *J. Polym. Sci. Part C: Polym. Sym.* **1973**, *42*, 817-832.

(64) Salammal, S. T.; Balandier, J.-Y.; Kumar, S.; Goormaghtigh, E.; Geerts, Y. H. Influence of Solubilizing Group Removal Rate on the Morphology and Crystallinity of A Diketopyrrolopyrrole-Based Compound. *Cryst. Growth Des*. **2014**, *14*, 339-349.

(65) Laudise, R. A.; Kloc, C.; Simpkins, P. G.; Siegrist, T. Physical Vapor Growth of Organic Semiconductors. *J. Cryst. Growth.* **1998**, *187*, 449-454.

(66) Biradha, K.; Santra, R., Crystal Engineering of Topochemical Solid State Reactions. *Chem. Soc. Rev.* **2013,** *42*, 950-967.

(67) Pappenfus, T. M.; Bashir, A.; Gerold, B. J.; Granaas, P. M.; Janzen, D. E. Synthesis, Characterization, and Electronic Properties of A Thermally-Labile Isoindigo. *J. Mol. Struct.* **2015**, *1095*, 96-99.

TOC

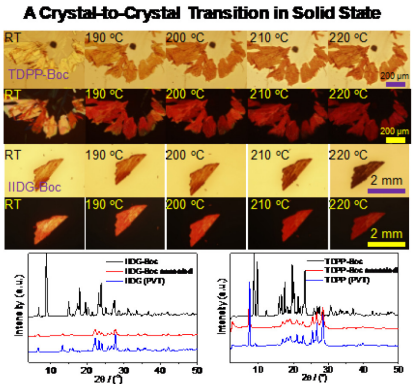
A Crystal-to-Crystal Transition in Solid State
RT
190 °C
200 °C
210 °C
220 °C
TDPP-Boc
200 μm
IIDG-Boc
2 mm
Intensity (a.u.)
2θ / (°)